China Instrument and Control Society
Instrumentation
OPEN ACCESS
*INSTRUMENTATION*, Vol. 13, No. 1, March 2026 https://doi.org/10.15878/j.instr.202600318

Article-Intelligent Detection & Fault Diagnosis

# Hybrid Deep Learning for Hydraulic Cylinder Fault Diagnosis under Complex Conditions via Multi-Source Signal Fusion

**Chen Yang[1], Jianwen Yan[1,4*], Yixiong Feng[2], Lei Li[3], Jianrong Tan[4]**

[1] School of Mechatronics Engineering, Anhui University of Science & Technology, Huainan 232000, China

[2] College of Mechanical Engineering, Guizhou University, Guiyang 550025, China

[3] Institute of Green Design and Manufacturing Engineering, Hefei University of Technology, Hefei 230009, China

[4] State Key Laboratory of Fluid Power and Mechatronic Systems, Zhejiang University, Hangzhou 310027, China

[*] Corresponding author email: 2025135@aust.edu.cn

**Abstract:** Hydraulic presses are indispensable in automotive and aerospace manufacturing, with hydraulic cylinders serving as key components for operational safety and product quality. Internal leakage faults in hydraulic cylinders are difficult to diagnose due to the scarcity of labeled data, the complexity of fault mechanisms, and the limited representation capability of single-signal methods under variable operating conditions. To address these issues, a hybrid deep learning feature fusion model based on displacement error and pressure signal, including convolutional autoencoder, multi-head attention mechanism, residual network and bidirectional long short time series neural network (CAEMRAB), is proposed for the diagnosis and classification of leakage faults in hydraulic cylinders. A hydraulic cylinder test system simulates heavy load, variable speed, and nonlinear motion under actual operating conditions. Through the all-round deep feature decoupling of the proposed model, the multi-source signal representation ability in complex and multi-noise environments is enhanced, effectively extracting the local and global features of displacement error and pressure signal fault data and achieving efficient classification. Experimental results indicate that the proposed model achieves at least a 3.95% improvement in diagnostic accuracy compared with ablation models. In addition, it exhibits high diagnostic stability across other models, single-signal diagnosis, varying sample sizes, and complex noise conditions. These experiments fully validate the superior performance of the proposed method in terms of diagnostic accuracy, reliability, and robustness.

**Keywords:** hydraulic cylinder; feature fusion; multi-source signal; hybrid deep learning; deep feature decoupling



**Citation:** Chen Yang, Jianwen Yan, Yixiong Feng, Lei Li, Jianrong Tan."Hybrid Deep Learning for Hydraulic Cylinder Fault Diagnosis under Complex Conditions via Multi-Source Signal Fusion." Instrumentation 13, no.1 (March 2026). https://doi.org/10.15878/j.instr.202600318

## 1 Introduction

Large, high-speed hydraulic machines have been widely adopted in production owing to their high efficiency, precision, and controllability[1]. As the core actuator of hydraulic machines, the stable operation of hydraulic cylinders guarantees production quality and safety[2,3]. However, faced with complex working conditions and production environments, the types and probabilities of hydraulic cylinder faults exhibit substantial diversity, concealment, and randomness, which increases the challenge of fault detection and diagnosis[4]. Therefore, in-depth research on efficient fault diagnosis schemes for hydraulic cylinders is crucial for enhancing production efficiency, ensuring operational

safety, and driving industrial progress.

Fault diagnosis technology for hydraulic cylinders was initially based on model-driven methods[5]. Reference [6] employed a model-based fault detection and isolation scheme, effectively enabling fault diagnosis in the rudder servo system for ship navigation. However, model-driven diagnostic methods are overly dependent on expert systems and precise modeling, and as system complexity increases, the difficulty of fault diagnosis rises dramatically. With advances in sensor technology, under a machine learning framework, Maddahi et al. [7] utilized data-driven methods to analyze the time and frequency domains of hydraulic cylinder pressure signals, achieving internal leakage fault detection; Jin et al. [8] extracted features using wavelet transforms and combined them with a wavelet neural network to classify faults caused by hydraulic cylinder seal damage. Nevertheless, the diagnostic accuracy of machine learning methods remains limited by expert knowledge and feature extraction techniques. Ma et al.[9] proposed a fault diagnosis strategy for solenoid valve groups based on current signals using a support vector machine, which enables both fault diagnosis and early warning. However, the traditional diagnostic accuracy of machine learning methods is still constrained by their dependence on expert knowledge and signal feature extraction techniques, which limit their ability to represent fault information and make it difficult to address the nonlinear relationships in long-sequence data of hydraulic cylinders. Therefore, with the advancement of models, further research is needed on how to better align intelligent models and architectures with diagnostic objectives while enhancing the representation capability of fault signals.

Currently, improvements in deep learning models[10], module integration[11,12], and hyperparameter optimization [13] have been extensively studied and widely applied. Convolutional neural networks (CNN), owing to their excellent feature learning capabilities, hold a significant position in the diagnosis of rotational faults [14]. However, CNN struggle to capture feature information in long time-series data fully. To address this, CNN are employed for local feature extraction, supplemented by long short-term memory (LSTM) to enhance the identification of long-term dependencies in the data, thereby improving training efficiency[15-17]. Ma et al. [18] incorporated an attention mechanism into the CNN-LSTM model, enabling the model to focus on valuable information in long-sequence data, which significantly enhanced its ability to predict faults in electro-hydraulic actuators. However, traditional CNN models rely heavily on labeled data, making it difficult to effectively address the diagnostic requirements for hydraulic cylinder systems' strongly nonlinear and concealed faults. Liang et al.[19] designed a Siamese Random Spatiotemporal Graph Convolutional Network, which demonstrated strong feature extraction capabilities in the fault diagnosis of hydraulic axial piston pumps. Snyder et al. [20] integrated one-dimensional and two-dimensional information and successfully applied it to bearing fault diagnosis. Wang et al. [21] transformed time series into two-dimensional data and developed a diagnosis model based on sparse attention, thereby improving both diagnostic efficiency and accuracy. Zeng et al. [22] combined autoencoders, attention modules, and LSTM models to achieve unsupervised dynamic fault detection. Deep learning models are effective in extracting fault features, but for long-period time series of hydraulic cylinders under heavy load and time-varying operating conditions, both one-dimensional data and image-transformed data remain difficult to process. In addition, fault data collection under such conditions is challenging, leading to limited sample sizes that are insufficient for the needs of deep learning models. Autoencoder-based methods also show limitations in capturing global features of highly nonlinear and latent long-sequence data in complex operating environments. Therefore, there is a need to explore combined models in which different modules can complement each other's shortcomings.

Data availability is also a crucial factor in determining fault diagnosis accuracy based on learning models. Due to their ease of measurement, vibration signals are widely used for fault diagnosis of various rotating components[23,24]. By decomposing [25], transforming[26] the signals, and combining them with different types of deep learning algorithm models, high-precision fault diagnosis and monitoring can be achieved. However, with the continuous development of equipment and the increasing complexity of working environments, relying solely on a single sensor signal makes it difficult to achieve precise fault diagnosis[27,28]. Consequently, complementary fusion models for multi-sensor signals have gradually become important for fault diagnosis. Information fusion schemes mainly include data-level fusion, feature-level fusion, and decision-level fusion[29,30]. Xiao et al. [31] constructed multi-layer graph data to achieve hierarchical fusion of multi-sensor information, employed convolution and graph convolutional networks for feature extraction, and finally applied a decision fusion strategy to accomplish fault classification. Yang et al. [32] designed a sparse Transformer, which first uses one-dimensional convolution to extract local features from multi-sensor data, then applies the Transformer to capture global features, and ultimately performs feature fusion to complete the classification task. Li et al.[33] extracted data features from three vibration sensors positioned at different locations and further performed compressor fault type diagnosis through feature concatenation. However, in the fault diagnosis of hydraulic systems, vibrations from different components can significantly interfere with the acquisition of fault-related vibration signals. Based on previous studies, research on homogeneous sensors has achieved promising results in the field of rotating machinery. In contrast, for hydraulic

cylinder fault diagnosis, discrepancies among sensor indicators increase data diversity, which in turn raises the difficulty of exploiting data complementarity[34-36]. Meanwhile, the characteristics of long-period time-series signals impose higher demands on the joint modeling of both global and local feature perception. Therefore, further experimental investigation is required on multi-sensor information fusion for fault diagnosis of hydraulic cylinders under complex operating conditions.

In summary, fault diagnosis of hydraulic cylinders under heavy load and time-varying operating conditions faces considerable challenges in both model development and signal data utilization. Traditional models primarily focus on learning features from a single signal or model structure, making it difficult to adapt to the complex long-sequence data of hydraulic cylinders. Although subsequent studies have enhanced feature extraction capabilities and employed signal fusion to compensate for model limitations, these approaches have been applied mainly to high-speed rotating machinery. Moreover, existing research often targets small-scale hydraulic cylinders or simplified experimental environments, leaving significant gaps in studies on heavy load and time-varying hydraulic cylinder fault diagnosis. In addition, the scarcity of long-period time-series data, the complexity of models required for joint extraction of local and global features, and the challenges in multi-sensor feature fusion further hinder progress in this field. To bridge these gaps, a multi-sensor monitoring test system for hydraulic cylinders under complex operating conditions was designed. Based on this system, the CAEMRAB fault diagnosis model is proposed to address the deep coupling of local and global features in long-sequence data under limited conditions.

The main contributions of this paper are as follows:

(1) A hydraulic cylinder internal leakage test rig was constructed under heavy load and time-varying operating conditions. Five leakage levels were designed, and multi-sensor signals were collected under different fault types, providing comprehensive data support and an experimental foundation for the proposed model in hydraulic cylinder fault diagnosis.

(2) A feature fusion algorithm model based on CAEMRAB was developed, which achieves deep coupling and fusion of multi-level features by comprehensively integrating local spatial features with global temporal dependencies.

(3) Comparative experiments with ablation models and other advanced models verified the high diagnostic accuracy of the proposed approach. Single-signal diagnostic comparisons demonstrated the effectiveness of the feature fusion strategy in handling the strong nonlinearity of hydraulic systems under complex conditions. Furthermore, experiments with varying amounts of labeled and unlabeled data evaluated the model's stability in practical scenarios with complex signal data. Finally, noise interference with different signal-to-noise ratios was introduced, confirming the effectiveness and robustness of the proposed feature fusion strategy across diverse operating conditions, and further demonstrating its engineering feasibility.

# 2 Methodology

## *2.1 Fault Type Analysis and System Establishment*

As shown in Fig. 1, the hydraulic cylinder, which serves as a core actuator in large-scale hydraulic press equipment, directly impacts production quality and safety. However, due to the complex structure and

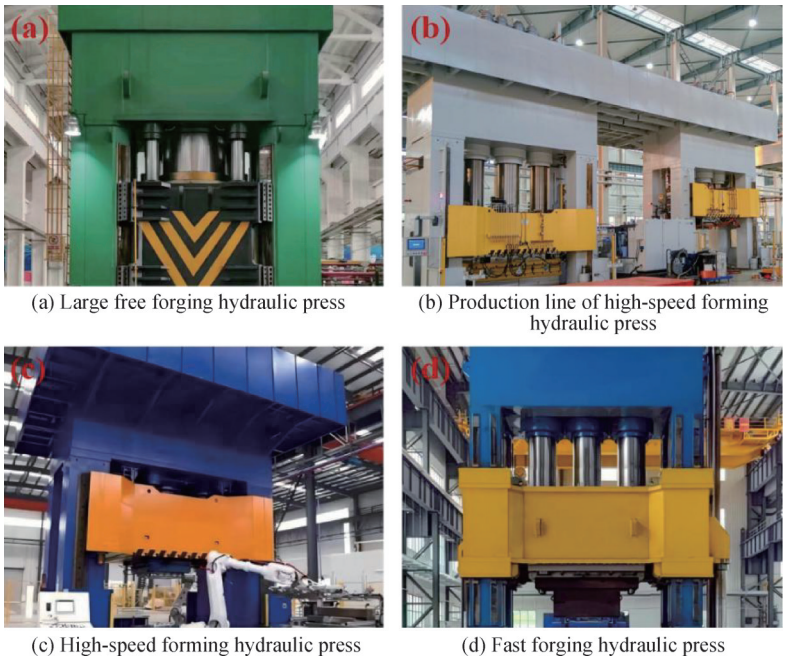


(a) Large free forging hydraulic press
(b) Production line of high-speed forming hydraulic press
(c) High-speed forming hydraulic press
(d) Fast forging hydraulic press

Fig.1 Complex application conditions of hydraulic cylinder (a. Large free forging hydraulic press; b. Production line of high-speed forming hydraulic press; c. High-speed forming hydraulic press; d. Fast forging hydraulic press)

concealed installation of the hydraulic systems in large hydraulic presses, it is difficult to identify fault promptly causes through visual inspection, and the effects of minor leakages on the cylinder's operating state are not readily apparent. Consequently, displacement and pipeline pressure sensors are essential for assessing the cylinder's condition. Nevertheless, given the complexity of the system and operating environment, as well as unavoidable signal interference, data from a single sensor are insufficient to characterize the hydraulic cylinder's operational status fully. In summary, the correlation and complementarity between displacement sensor data and pressure signals can effectively facilitate the diagnosis of hydraulic cylinder faults.

Under heavy load and variable-speed conditions, large hydraulic presses are extremely sensitive to even minor changes in system operation, which can lead to irreversible structural damage and leakage faults in the hydraulic cylinders resulting. Furthermore, because the hydraulic cylinders used in large hydraulic presses are relatively large, with high material performance requirements and production quality that is difficult to control fully, subtle damage to the cylinder may go unnoticed; once the cylinder structure is compromised, prolonged operation can cause wear or breakage of components such as sealing rings. As the core actuator of large hydraulic presses, hidden internal leakage faults in hydraulic cylinders seriously threaten production safety, equipment operation, production efficiency, and product yield. Therefore, identifying the types of hidden internal leakage faults in large hydraulic presses is a key initial condition for advancing fault diagnosis in hydraulic cylinders under heavy load and complex operating conditions. Fig. 2 illustrates the various hydraulic cylinder fault types commonly observed in production operations.


Fig.2 Internal leakage fault types in engineering practice

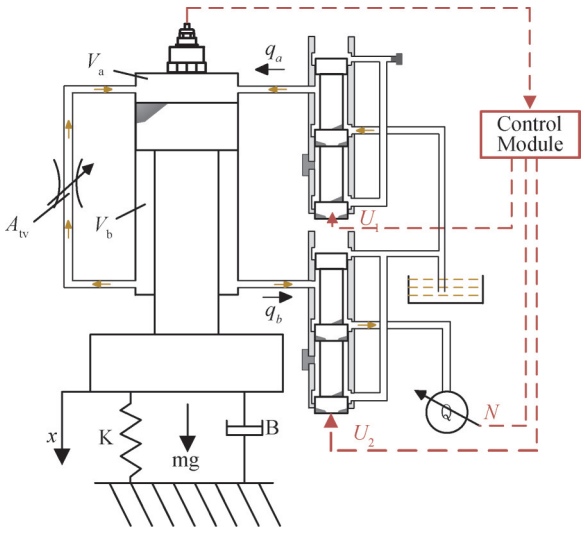


Fig.3 Fault operation principle

As shown in Fig. 2, different fault types cause varying leakage flow rates. Accordingly, Fig. 3 illustrates the fault principles and motion process. Under heavy load conditions, the rod chamber of the hydraulic cylinder remains in a high-pressure state, and for all fault types, the hydraulic fluid leaks from the rod chamber to the non-rod chamber. During the downward movement of the moving beam, displacement closed-loop control is adopted to collect displacement error and rod chamber pressure data under variable-speed conditions with different leakage rates. When the moving beam returns, a servo motor ensures constant flow control. The controller sets the movement's start and end conditions, and the servo valves for both the rod chamber and non-rod chamber circuits are fully opened to minimize the instability caused by valve regulation.

Considering the safety of personnel and the experimental environment, an external throttle valve is used to simulate the leakage failure in the upper and lower cavities of the hydraulic cylinder. As shown in Equation (1), according to the pressure difference of the loop servo valve in the upper and lower cavity of the hydraulic cylinder and the size of the throttle valve opening in the middle cut-off state, the leakage flow in the hydraulic cylinder under six different throttle opening degrees is calculated by using the orifice flow model. Combined with the actual operation characteristics of different hydraulic cylinder fault states, the leakage amount and corresponding fault types are shown in Table 1.

Table 1 Leakage and failure types

| Type code | #0 | #1 | #2 | #3 | #4 | #5 |
|---|---|---|---|---|---|---|
| Leakage (L/min) | 0 | 0.39 | 0.78 | 1.17 | 1.56 | 1.94 |
| Fault type | Normal | Piston wear | Wear of the sealing ring | Cylinder block break | Sealing ring break | Sealing ring loss |

$$Q_{\text{leak}} = k * A_{\text{tv}} * \sqrt{\Delta P} \quad (1)$$

where, $Q_{\text{leak}}$ represents the flow through the throttle valve leakage; $k$represents the experience coefficient; $A_{\text{tv}}$represents the opening area of the throttle valve; $\Delta P$ indicates the pressure difference between the two ends of the throttle valve (that is, the pressure difference between the upper and lower chambers of the hydraulic cylinder).

## 2.2 Construction of the Proposed Model

For the hydraulic cylinder motion model under heavy load and variable-speed conditions, the single-cycle signals are lengthy and complex, with insufficient labeled data across different operating conditions and a limited ability of single sensors to clearly capture fault features. As illustrated in Fig. 3, when an internal leakage fault occurs in the hydraulic cylinder, both the pressure in the dual chambers and the displacement tracking state change, indicating a strong correlation between these signals and the fault state. Consequently, the system adopts a closed-loop displacement control scheme, causing the displacement data to exhibit time-varying and nonlinear characteristics that better meet production requirements. Additionally, built-in displacement sensors that are directly linked to system variables and pressure sensors located in the high-pressure chamber loop are employed to collect sensor data under various leakage conditions. To ensure that the data fully capture fault features, data spanning more than four motion cycles are grouped together, and both pressure and displacement error data are extracted.

Secondly, a dual-channel feature extraction model based on the autoencoder is established. Unlike traditional methods, the encoder further integrates a multi-head attention mechanism, a residual connection network, and a Bidirectional Long Short-Term Memory (BiLSTM) module, which enable efficient extraction of local and global features from the two signals through hierarchical integration of global information. This model not only inherits the advantages of convolutional autoencoders in local feature extraction and neuron weight sharing, but also significantly enhances feature capture through the synergy of its modules, ultimately achieving effective feature fusion and fault classification. The overall structure of the proposed model is shown in Fig. 4.

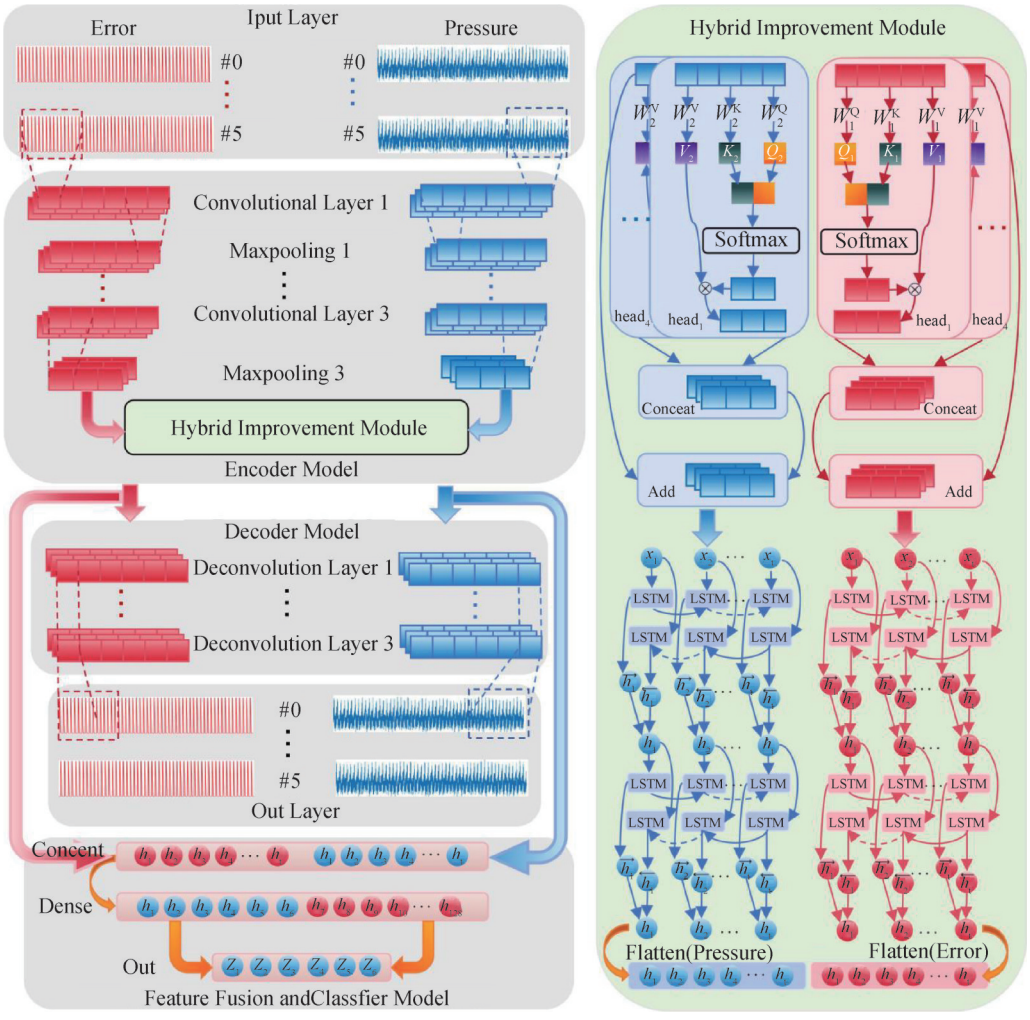


Fig.4 Overall structure of the proposed model

### 2.2.1 Encoder Module

The proposed model's autoencoder module comprises three convolutional layers, three pooling layers, one multi-head self-attention network, a residual connection module, and two BiLSTM layers. For the dual-channel inputs of displacement error signals, and pressure signals, two parallel convolutional layers are constructed to capture local features in the time series, while the pooling layers further reduce the length of the time-series data. This enables the model to focus more on critical features and enhances the selectivity of the filters, thereby extending the applicability of feature detection, as illustrated in Equation (2).

$$\begin{cases} h_i^l = f\times\left(X_i * W_i^l + b_i^l\right) \\ Y_i^{l+1} = \max\left(h_i^l\right) \end{cases} \tag{2}$$

where, $h_i^l$denotes the feature output of the layer $l$after convolution; $f$denotes the activation function; $X_{\mathrm{i}}$ denotes the input data; $W_i^l$denotes the weight matrix of the convolution kernel; $b_i^l$denotes the bias term; $Y_i^{l+1}$denotes the output feature element of the layer$l+1$after max pooling; $max$denotes the max pooling operation; $i$denotes the identifier for the corresponding channel signal input.

As shown in Fig. 4, the proposed model employs a multi-head attention mechanism that performs parallel computations across its attention heads, enabling each head to focus on information from different subspaces. The resulting outputs are then concatenated to yield a richer feature representation, effectively preventing the loss of critical latent details[37,38]. As shown in Equation (3), each attention head within the multi-head self-attention mechanism performs a weighted computation on the time-series features produced by the final pooling layer, and the weights are normalized using the softmax function to ensure that the sum of the attention scores equals 1. Equation (4) shows that the multi-head self-attention mechanism further improves the model's feature representation capability by concatenating all attention-head outputs.

$$\begin{cases} Q_i = Y_i^{l+1} W_i^Q,\ K_i = Y_i^{l+1} W_i^K,\ V_i = Y_i^{l+1} W_i^V \\ \text{Self}-\text{Attention}(Q_i, K_i, V_i) = \text{softmax}\left[Q_i K_i^T \Big/ \sqrt{d_k}\right] V_i \end{cases} \tag{3}$$

$$\begin{cases} \text{MA}(Q_i, K_i, V_i) = (\text{head}_1, \cdots, \text{head}_h) W_{oi} \\ \text{head}_h = \text{Self}-\text{Attention}(QW_i^Q, KW_i^K, VW_i^V) \end{cases} \tag{4}$$

where, $Y_i^{l+1}$denotes the input sequence; $W_i^Q$, $W_i^K$, $W_i^V$denotes the weight matrix; $Q_i$ denotes the query matrix; $K_i$denotes the key matrix; $V_i$denotes the value matrix. $W_i^Q$, $W_i^K$, $W_i^V$denote the corresponding parameters of the respective attention heads; $W_{oi}$denotes the output weight matrix and $h$ denotes the number of attention heads.

To prevent information loss when processing nonlinear, time-varying, and long time-series data in hydraulic cylinders, this study employs a residual network to effectively fuse the feature information conveyed by the multi-head attention mechanism with the initial features provided by the encoder model, thereby enhancing the integrity of the information and ensuring that critical data are not omitted. This fusion layer can capture global dependencies more comprehensively, thereby effectively avoiding issues such as information loss and gradient vanishing [39-41].

$$Z_{\text{out},i} = Y_i^{l+1} + \text{Multi}-\text{Head Self}-\text{Attention}(Q_i, K_i, V_i) \tag{5}$$

where, $Z_{\text{out},i}$denotes the feature output after residual connection processing; $Y_i^{l+1}$the feature output of the encoder model; $Q_i$, $K_i$and $V_i$ the feature output after being weighted by the multi-head self-attention mechanism.

As shown in Fig. 4, to effectively address the gradient vanishing and exploding issues encountered during the processing of long time-series data, a BiLSTM network was introduced. This network model adopts forward and backward LSTM structures that process the bidirectional time-series data flow from past to future and from future to past respectively, then merges the outputs from both layers to enhance the model's capability in handling the interdependencies of sequential data [42,43]. Based on the LSTM information propagation and parameter update formulas, the forward hidden state $\overrightarrow{h_{\mathrm{t}}}$ is computed, and the reverse hidden state $\overleftarrow{h_{\mathrm{t}}}$ is obtained by processing the input sequence in reverse order. Finally, the forward and reverse hidden states are concatenated to form the BiLSTM model, as shown in Equation (6).

$$h_{\mathrm{t,i}} = [\overrightarrow{h_{\mathrm{t,i}}}, \overleftarrow{h_{\mathrm{t,i}}}] \tag{6}$$

where, $h_{\mathrm{t}}$ denotes the final output of the BiLSTM model; $\overrightarrow{h_{\mathrm{t}}}$ denotes the forward hidden state;$\overleftarrow{h_{\mathrm{t}}}$ denotes the reverse hidden state.

### 2.2.2 Deconvolution Decoder

The decoder module expands the feature parameters extracted from the encoder through three deconvolution layers to reconstruct the sample data. The up sampling-based feature expansion and reconstruction effectively reduce noise interference in the original data, as shown in Equation (7).

$$\tilde{X}_i = f\times\left(\sum_{j=1}^{H} Z_{\text{out},i} * W_i^{IT} + c_i^l\right) \tag{7}$$

where, $\tilde{X}_i$represents the reshaped sample data; $f$represents the deconvolution activation function; $Z_{\text{out},i}$represents the decoder input; $W_i^{IT}$represents the transposed convolution kernel matrix; and$c_i^l$ represents the bias term.

The autoencoder model aims to compress sample data features, extract key local features, extract important local features, and reconstruct the sample data through the decoder to reduce the difference between the original data and the reconstructed data, effectively reducing the noise impact of the original sample data. To achieve this goal, the loss function uses mean squared error, as shown in Equation (8).

$$L_{\text{MSE}} = \sum_{i=1}^{T}\sum_{j=1}^{C}\left(X_{i,j} - \tilde{X}_{i,j}\right)^2 \Big/ (T\times C) \tag{8}$$

where, $L_{MSE}$ denotes the loss function, $T$ denotes the number of time steps, $C$ denotes the characteristic number, $X_{i,j}$ denotes the original sample data, $\tilde{X}_{i,j}$ denotes the reconstructed sample data.

### 2.2.3 Feature Fusion and Classification Module

Due to the strong nonlinearity, time-varying nature, high concealment, and difficulties in feature extraction associated with hydraulic component faults, the diagnostic challenge increases accordingly. Relying solely on a single sensor for accurate fault diagnosis is also highly challenging. As shown in Fig. 5, signals are collected using various equipment sensors to obtain the data set, $\boldsymbol{Data}_t$, which is then preprocessed and fused using different approaches to integrate multi-source sensor information. Information fusion is generally classified into data-level fusion, feature-level fusion, and decision-level fusion. Hydraulic fault diagnosis relies on diverse signal sources; directly acquiring these signals is extremely complex. Under the influence of strong noise, external signals fail to reflect the operating condition of hydraulic components adequately. Therefore, under heavy load and variable-speed conditions, a feature-level information fusion strategy is employed to accurately represent the working state of the hydraulic cylinder through comprehensive feature integration to diagnose internal leakage faults in hydraulic cylinders.

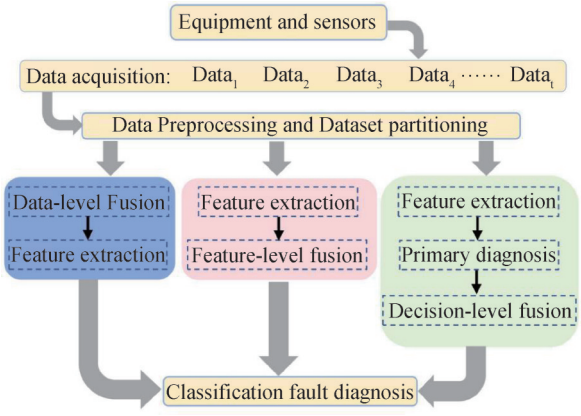


Fig.5 Information fusion strategy

Based on this, all of its parameters are frozen after the feature extraction module has been trained. The classification model first fuses the features extracted from the two sensor signals and then completes the classification task using a fully connected layer and an activation function, as shown in Equation (9).

$$\begin{cases} Input_{\text{classifier}} = Concat\left(Out_{\text{error}}, Out_{\text{pressure}}\right) \\ den = f_{\text{den}}\left(W_{\text{den}} \cdot Input_{\text{classifier}} + b_{\text{den}}\right) \\ out = f_{\text{out}}\left(W_{\text{out}} \cdot den + b_{\text{out}}\right) \end{cases} \tag{9}$$

where, $Out_{\text{error}}$ and $Out_{\text{pressure}}$ denote the output features of the extracted displacement error and pressure signal, respectively; $Concat$ denotes the feature fusion connector; $Input_{\text{classifier}}$ denotes the classifier input after feature fusion; $den$ denotes the output of the fully connected layer; $f_{\text{den}}$ denotes the activation function of the fully connected layer; $W_{\text{den}}$ and $W_{\text{out}}$ denote the weights of the fully connected layer and the output layer, respectively; $b_{\text{den}}$ and $b_{\text{out}}$ denote the biases of the fully connected layer and the output layer, respectively; $out$ denotes the output of the output layer; and $f_{\text{out}}$ denotes the activation function of the output layer.

# 3 Case Study

## *3.1 Fault Type Analysis and System Establishment*

To verify the effectiveness of the proposed model, an experimental test rig was constructed, as shown in Fig. 6. The setup primarily consists of a hydraulic station, valve block platform, leakage simulation device, hydraulic press, control station, and power cabinet. The hydraulic station comprises an oil tank, servo motor, accumulator, and vane pump, providing hydraulic power to the system. The independent control servo valves for the upper and lower chambers of the hydraulic cylinder are mounted on the valve block platform, enabling variable-speed closed-loop displacement control. The test rig adopts a four-column structure, with a high-mass sliding block to simulate heavy-load motion scenarios in industrial production, enhancing the applicability of internal leakage fault diagnosis under heavy-load conditions.

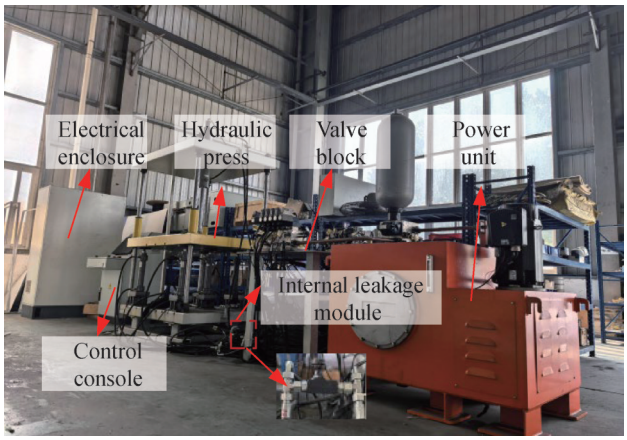


Fig.6 Configuration and control model of experimental equipment

The leakage simulation device connects to the hydraulic cylinder's upper and lower chambers via a three-way connector, throttle valve, and hose, allowing experiments with varying leakage levels. The control station consists of a host computer, data acquisition card, and output card, utilizing the Simulink platform for real-time data acquisition and closed-loop control signal output. The power cabinet supplies high-voltage and electrical power to the control station, system, and servo motor, ensuring the stable operation of the test rig. Based on experimental requirements, the main hydraulic and electronic components involved in signal generation and acquisition in the test rig are listed in Table 2.

Table 2 Main components and main parameters of the test bench

| Component | Model Number | Main Parameters | |
|---|---|---|---|
| Pressure sensors | HM20-2X/400-C-K35 | Measurement range | 0-40Mpa |
| Hydraulic Cylinder | HSG03-100/70-H4110-600 | Bore Diameter | 100mm |
| | | Rod Diameter | 70mm |
| | | Stroke | 0-600mm |
| Built-in Displacement Sensor | Forever7.1-1-2-0340-1-AI0 | Working Range | 25-600mm |
| Analog signals input card | PCI-1713 | Maximum Acquisition Frequency | 10kHz |
| Analog signals output card | NI PCI-6703 | Maximum Output Frequency | 350kHz |
| Digital signals input/output card | PCI-1751U | Maximum Acquisition/Output Frequency | / |

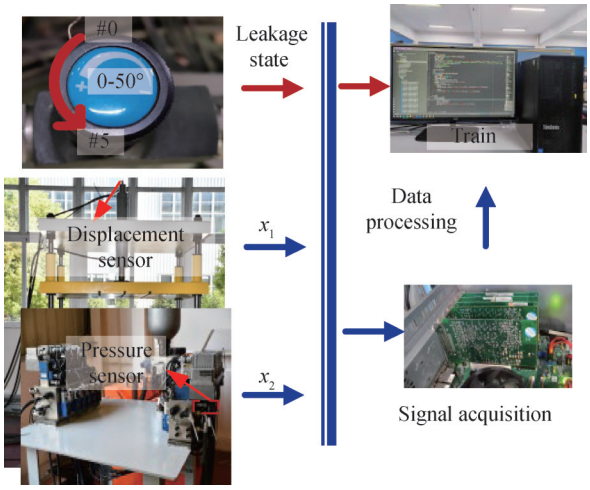


Fig.7 Signal acquisition and training

As shown in Fig. 7, small hole leakage models in different states as shown in Fig. 3 are created by rotating the Angle of the throttle valve. Subsequently, the required signals $X_1$ and $X_2$ in Eq. (2) are collected by the displacement and pressure sensors, the leakage status of the throttle valve is obtained by the computer and the pre-processed sensor data is obtained. Finally, the goal of model training and diagnosis is realized.

As illustrated in Fig. 8a, the time-varying speed characteristics of the motion curve and the impact of high noise reduce the sensitivity of fault features in the data, thereby increasing the difficulty of normalization and feature extraction. Therefore, by taking advantage of the benefits of closed-loop displacement control, the displacement error data generated by the difference between the actual displacement and the theoretical displacement is used as one of the fault feature extraction signals for the model channel, as shown in Fig. 8b. During operation, leakage causes significant pressure changes in the high-pressure chamber; thus, the pressure signal from the high-pressure chamber is employed for fault classification, as evidenced by the single-cycle pressure signal shown in Fig. 8c. Furthermore, as depicted in Fig. 9, data for six different leakage levels are collected, with 76 cycles acquired for each category.

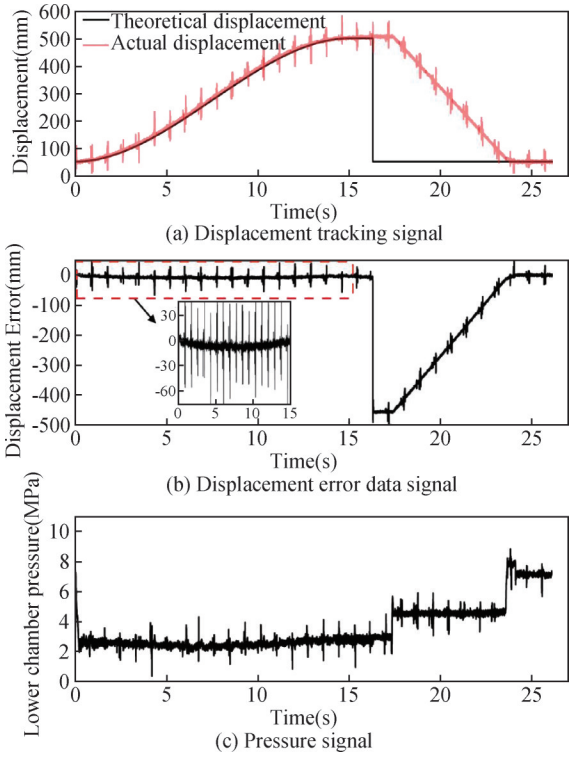


Fig.8 Graph of single-cycle motion signals in normal state: (a) Displacement tracking signal; (b) Displacement error data signal; (c) Pressure signal

As shown in Fig. 9, under a high-noise environment, the two signals in the initial leakage state for cases #0 and #1 are difficult to differentiate effectively; the displacement error signals for cases #1 and #2 are hard to distinguish, whereas the pressure signal exhibits significant changes; and for cases #3 and #4, the displacement error signals show only minor variations, while the pressure signal is not clearly distinguishable. In summary, the fault expression capability is enhanced by effectively exploiting the complementary differences between displacement error and pressure signals, thereby providing a solid foundation for fault diagnosis.

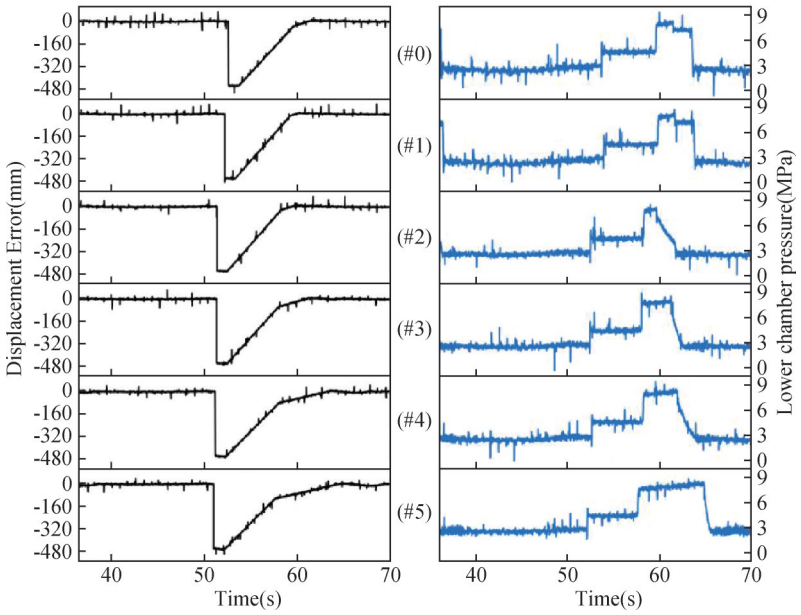


Fig.9 Single-cycle dataset of six types of state displacement errors and pressure signals

### *3.2 Experimental Design and Evaluation Metrics*

To independently evaluate the contribution of each module to the overall diagnostic performance and thereby validate the rationality of the proposed fusion strategy, ablation models were designed based on the innovative structural modules of the model. CAERB: the multi-head attention module is removed. CAEMR: the BiLSTM module is removed. CAEMB: the residual connection module is removed. CAEB: both the multi-head attention and residual connection modules are removed. CAE: all module concatenations are removed, leaving only the convolutional autoencoder. Furthermore, in view of current research progress, CNN[14], CNN-LSTM[18], Graph Attention Networks (GAT), Transformer[32], and Informer[44] models were introduced as comparative baselines to further demonstrate the effectiveness of the proposed model.

For training, the proposed model and its ablation variants were trained in an unsupervised manner using 12, 000 unlabeled samples, generated from 6 types of pressure signals and six types of displacement error signals (1, 000 samples each), with 10% of the data reserved for validation to train the convolutional autoencoder. Subsequently, supervised training of the feature fusion and classifier modules was performed using a labeled training set of 6, 000 samples (500 samples per signal type), again with 10% for validation. Finally, a test set of 2,400 samples (200 per signal type) was used for model evaluation. The comparative models (CNN, CNN-LSTM, GAT, Transformer, and Informer) were trained and evaluated under the same data settings as the proposed model and its ablation variants.

The basic parameters of each layer in the proposed model are listed in Table 3. All models were executed in Python 3.10 on Windows 10 with 32.0 GB RAM, an Intel i5-12500 3.0 GHz processor, and an NVIDIA 3060 GPU. The learning rate for all models was set to 0.001, the step

Table 3 Parameters of each layer of the proposed model

| Module | Structure | Parameter | Value |
|---|---|---|---|
| Encoder | Input | Pressure/Displacement errors | (16834,1)/ (16834,1) |
| | Conv1D | Kernel_size | 128*4/128*4/64*4 |
| | | Strides | 4 |
| | Multi-Head Self-Attention | Heads | 4 |
| | | Key-dim | 64 |
| | MaxPooling1D | Pool-size | 2 |
| | Bilstm | Units | 128 |
| Decoder | Conv1DTranspose | Kernel_size | 128*4/128*4/64*4 |
| | Dense | Units | 128 |
| Classifier | Dense | Units | 128 |

size to 100, and the number of training epochs to 100. The convolutional, multi-head self-attention, and BiLSTM layers in the ablation models were configured identically to those in the proposed model. The CNN and CNNB models primarily consist of two convolutional layers, two pooling layers, and one fully connected layer. For these models, the convolutional kernels are all 64×4 with a stride of 4, the pooling size is 2, and the fully connected layer contains 64 units. Due to the larger parameter size of the Transformer, GAT, and Informer models, directly training them on the aforementioned hardware was challenging. To address this, a CNN layer with a 64×4 kernel was added before these modules to reduce the dimensionality of the long-sequence input signals.

The objective of this study is to maximize the diagnostic and classification performance for leakage faults in hydraulic cylinders. Guided by this goal, in order to comprehensively evaluate model performance, precision, recall, and F1-score were employed in addition to classification accuracy. These supplementary metrics help to avoid potential bias caused by relying on a single evaluation criterion and provide a thorough assessment of the model's effectiveness under experimental conditions. The definitions of these metrics are given in Equation (10).

$$\begin{cases} Accuracy = \dfrac{TP+TN}{TP+FP+TN+FN} \\ Precsion = \dfrac{TP}{TP+FP} \\ Recall = \dfrac{TP}{TP+TN} \\ F1score = 2 \times \dfrac{Precsion \times Recall}{Precsion + Recall} \end{cases} \tag{10}$$

where, *TP* (True Positive) denotes the number of samples correctly identifying the classification as positive; *TN* (True Negative) is the number of samples correctly identifying the classification as negative; *FP* (False Positive) is the number of samples incorrectly identifying the classification as positive; and *FN* (False Negative) is the number of samples incorrectly identifying the classification as negative.

### *3.3 Results and Discussions*

#### 3.3.1 Comparison of Ablation Experiment Results

Fig. 10 presents the diagnostic evaluation metrics of the proposed model and its ablation variants under the multi-source signal feature fusion strategy. As shown, the proposed model consistently outperforms conventional models across all evaluation metrics. Specifically, under the feature fusion strategy, the proposed model achieves a diagnostic accuracy and other metrics of 99.92%, representing a 3.92% improvement over the best performing comparative model. The results from the CAE ablation model indicate that the orderly combination of modules contributes to superior diagnostic performance. The integration of multi-head attention and residual networks ensures that features from multiple subspaces are effectively captured, providing a solid foundation for feature extraction by the BiLSTM module. Comparisons with the ablation models further demonstrate that the proposed model exhibits exceptional diagnostic capability for hydraulic cylinder leakage data, particularly under strong time-varying, nonlinear, and long-sequence conditions.

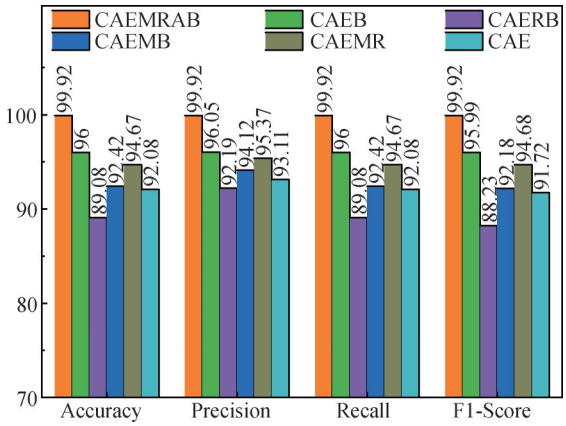


Fig.10 Comparison of evaluation metrics for ablation models under the feature fusion strategy

As shown in Fig. 11(a), the proposed model achieves high classification performance across all six fault types. Figs. 11(b) -11(f), representing the ablation models, exhibit considerable misclassification in tasks involving subtle leakage faults, such as piston rod and guide ring wear. The confusion matrices further indicate that, for hydraulic cylinder fault diagnosis under strong time-varying and nonlinear conditions, there remains room for improvement. Compared with the ablation models, the proposed model effectively handles the coupling between adjacent fault states, resulting in superior classification performance.

Fig. 12 presents visualizations of the classification outputs for different models. Fig. 12(a) shows that the proposed model achieves large inter-class separation, clearly distinguishing between different fault types. Figs. 12(b)-12(d) and Figs.12(e)-12(f) highlight the importance of the BiLSTM module in handling long-period time-series data, as it effectively increases inter-class distances. However, compared with the proposed model, all ablation variants exhibit classification issues, which hinder the efficient diagnosis of hydraulic cylinder faults in long-sequence data. Therefore, Fig. 12 provides a more intuitive demonstration that the proposed model achieves higher classification effectiveness for hydraulic cylinder internal leakage faults under heavy load and time-varying operating conditions.

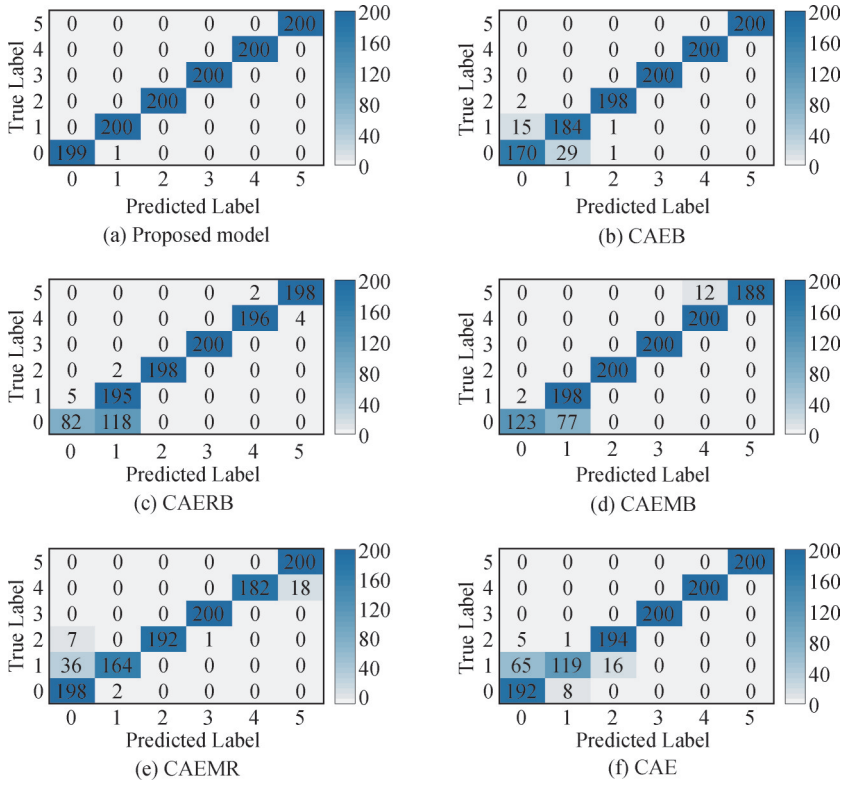


Fig.11 Confusion matrices of ablation models under the feature fusion strategy

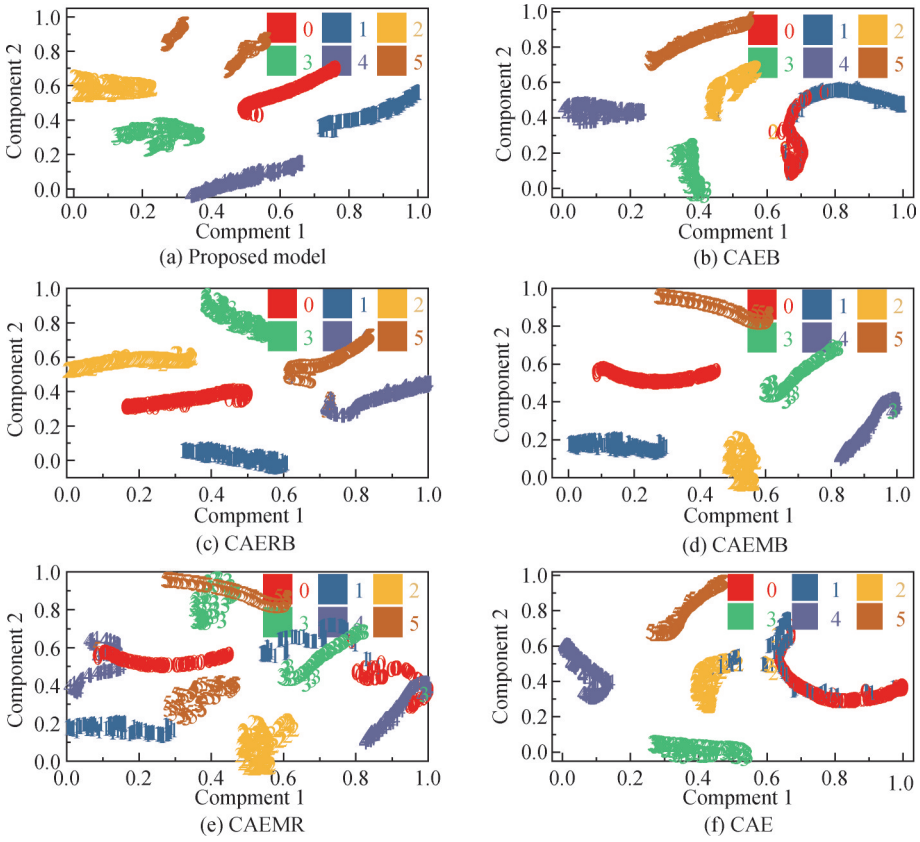


Fig.12 Visualization of classification results for ablation models under the feature fusion strategy

### 3.3.2 Comparison of Experimental Results with Other Models

As shown in Fig. 13, under identical data and experimental conditions, the proposed model achieves more effective and accurate fault diagnosis of hydraulic cylinders for long-period time-series data under heavy load and time-varying operating conditions, with an

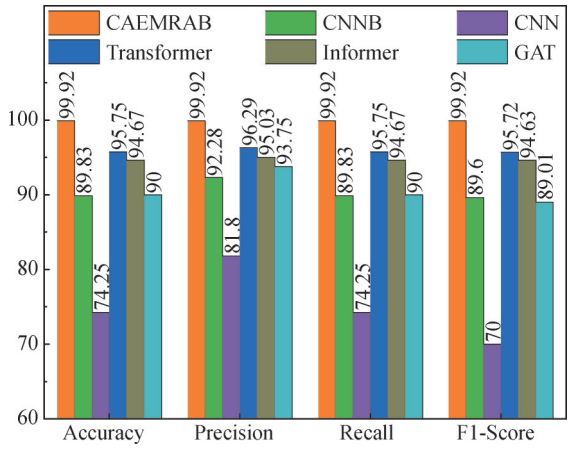


Fig.13 Comparison of evaluation metrics with other models under the feature fusion strategy

accuracy improvement of 4.17% over the best-performing comparative model. Fig. 14 indicates that the comparative models struggle to achieve adequate inter-class separation in classification tasks, whereas the proposed model demonstrates a clear advantage in this regard

From the CNN model, it is evident that traditional convolutional networks face considerable difficulty in extracting features from long-period time-series data. The Transformer and Informer models show clear advantages for long-sequence data compared to other baseline models; however, Fig. 14 reveals that their inter-class separation in classification still leaves room for improvement, with a noticeable gap relative to the proposed model. The GAT model, widely applied in fault diagnosis, performs well for high-frequency signals but exhibits certain limitations in the present experiments.

Overall, the comparative experiments further confirm that effective design of experimental modules tailored to the data characteristics is essential for fault diagnosis tasks in complex hydraulic cylinder operating environments.

### 3.3.3 Comparison of Feature Fusion Strategy and Single Signal Experimental Results

To investigate the effectiveness of the feature fusion strategy, the proposed model was used to perform classification evaluations separately on the displacement error and pressure datasets. In the single-signal fault diagnosis tasks, the experimental training data comprised 1000 groups of unlabeled data for each type of displacement error signal and pressure signal. In contrast, under the feature fusion strategy, the unlabeled and labeled training sets consisted of 12000 data groups, with 1000 groups per signal type. (CAEMRAB-E is the model for training displacement error signals, and CAEMRAB-P is the model for training pressure signals).

As shown in Figs. 15a and 15c, when the guide ring break or was lost, resulting in a large leakage, the displacement error signal gradually becomes insufficient to distinguish fault types, whereas under conditions of micro-leakage caused by piston rod and guide ring wear, the diagnostic performance of the pressure signal data is

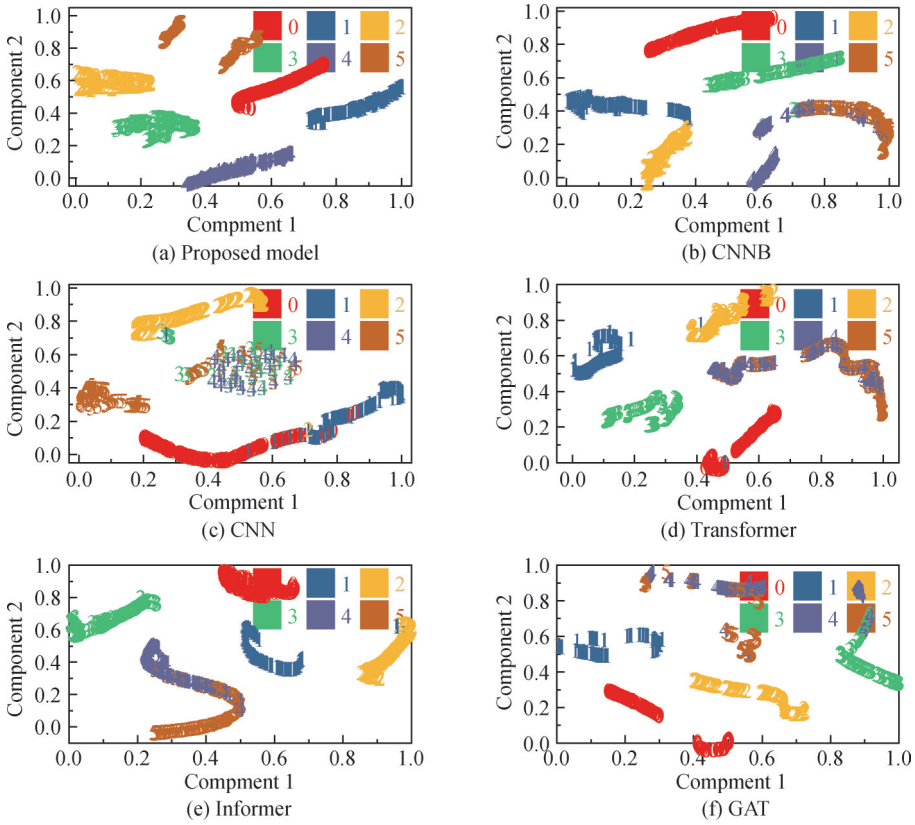


Fig.14 Visualization comparison with other models under the feature fusion strategy

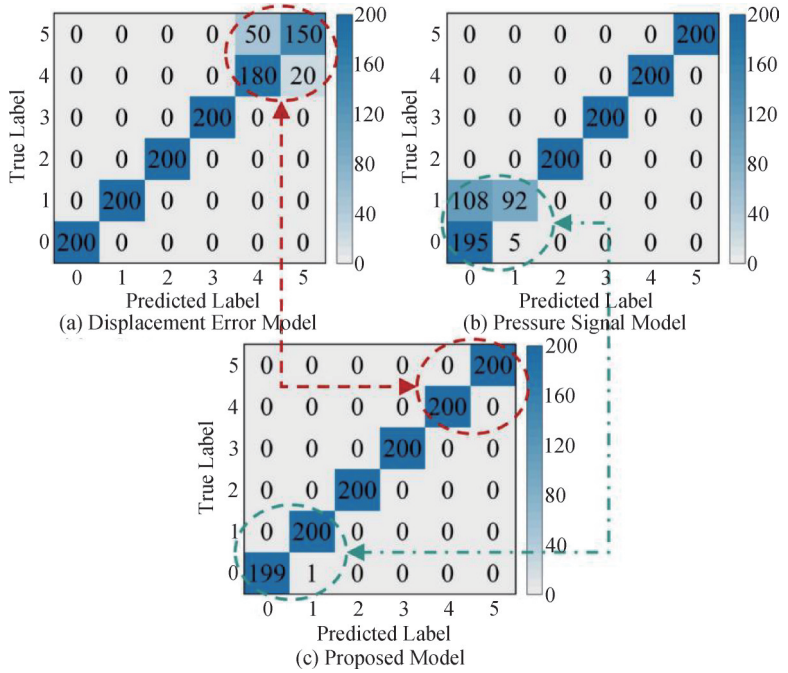


Fig.15 Confusion matrix of the proposed model under single signal and feature fusion strategy

relatively poor. Compared to a single signal, the feature fusion strategy used in Fig. 15c achieves a higher diagnostic accuracy and effectively distinguishes various fault types. This result further demonstrates the complementarity and differences between displacement error signals and pressure signals, as shown in Fig. 8. Analysis of Fig. 16 reveals that, in hydraulic cylinder fault diagnosis, the diagnostic performance based on pressure signal data is 3.59% lower than that based on displacement error signal data, indicating certain limitations in the ability of pressure signals to convey fault information. Moreover, intuitive analysis shows that the diagnostic performance after feature fusion is 5.75% higher than the best diagnostic result obtained using a single signal.

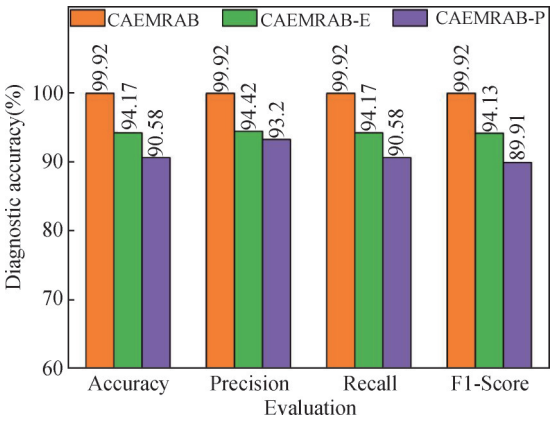


Fig.16 Comparison of four evaluation metrics for single signal and feature fusion strategies

Figs. 15 and 16 demonstrate that the feature fusion strategy outperforms the single-signal model in fault diagnosis tasks. The feature fusion approach effectively leverages the correlation and complementarity among signals collected by different sensors, compensating for the shortcomings of single-signal diagnostics under both micro-leakage and high-leakage conditions, thereby significantly enhancing the diagnostic accuracy for internal leakage faults in hydraulic cylinders. Moreover, the proposed algorithm model demonstrates strong fault diagnosis capabilities across different signal sources in the comparative study, thereby confirming its excellent robustness.

### 3.3.4 Comparison of Experimental Results With Different Sample Sizes

To further assess the feature extraction and diagnostic classification capabilities of the proposed model for multi-source signal fusion in hydraulic systems, comparative experiments were designed under varying conditions of labeled and unlabeled data. In the experimental validation, the training sets were composed of six types of pressure and displacement signals, with unlabeled data available in amounts of 800, 700, 600, and 300 groups, and labeled data available in amounts of 500, 400, 300, 200, and 100 groups, respectively, combined freely.

As shown in Fig. 17, the model diagnosis accuracy shows a significant positive correlation with the increase of marker data. When the marker data reaches 400, the model diagnostic effect is significantly improved, revealing the importance of marker data for differential fault learning. Secondly, the results of the proposed model under the same marker data comparison group show a strong stability of diagnostic performance. This finding further reveals the stability advantage of the proposed method under data distribution perturbation. It

provides a basis for the study of the number of small sample data on fault diagnosis accuracy.

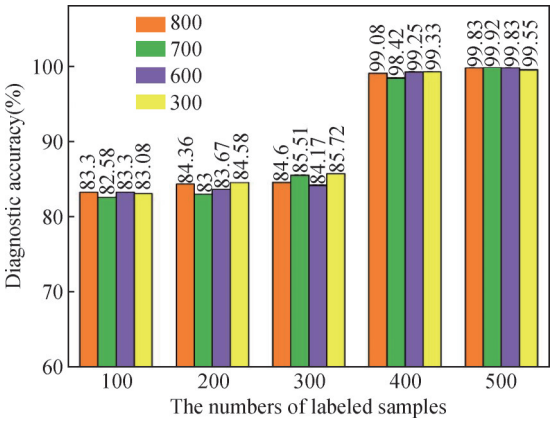


Fig.17 Diagnostic accuracy of the model for different labelled and unlabelled data

### 3.3.5 Comparison of Experimental Results Under Different Noise Levels

Due to the diverse application environments of different products, the noise form of the signals also has some differences. Therefore, this subsection adds Gaussian white noise based on the original signal noise to further enhance the interference of noisy data and simulate the signal form under different extreme signal-to-noise ratio conditions. The SNR are -3 dB, 3 dB, 6 dB, and 9 dB, and the SNR is calculated as in Equation (11).

$$SNR = 10*lg(P_S/P_N) \tag{11}$$

where, $P_S$ denotes the signal power and $P_N$ denotes the noise power.

As shown in Table 4, the proposed model consistently maintains a high diagnostic accuracy of over 98% under different SNR conditions, further demonstrating its stability and generalizability across varying operating environments. Compared with the ablation models and benchmark models, the proposed model improves diagnostic accuracy by at least 2.33% and 8.32%, respectively. The ablation models also achieve overall higher accuracy than other advanced models, validating the effectiveness of the proposed module combinations in hydraulic system fault diagnosis. Among the advanced models, the Informer exhibits notable advantages in handling long-sequence data and demonstrates relatively stable diagnostic performance under noisy conditions. These comparisons highlight the considerable challenges posed by hydraulic cylinder fault diagnosis under heavy load and time-varying operating conditions. Furthermore, the feature-fusion model achieves significantly higher accuracy than single-sensor approaches, with at least a 10% improvement under identical conditions. Experimental results across different noise levels further confirm the superior robustness of the proposed method under complex working environments.

Table 4 Diagnostic accuracy of each model under noise interference

| Model | Diagnostic accuracy | | | |
|---|---|---|---|---|
| | -3 | 3 | 6 | 9 |
| CAEMRAB | 98.75 | 98.24 | 99.83 | 99.42 |
| CAEB | 96.42 | 95 | 96.67 | 95.83 |
| CAERB | 83.58 | 83.50 | 85.75 | 87.50 |
| CAEMB | 86.42 | 89.83 | 87.08 | 89.58 |
| CAEMR | 78.33 | 86.42 | 84.75 | 93.67 |
| CAE | 92.67 | 93.92 | 95.75 | 92.92 |
| CNNB | 82 | 83.83 | 86.08 | 90.16 |
| CNN | 73.08 | 78.17 | 80.67 | 91.92 |
| Transformer | 81.33 | 84.75 | 87.42 | 92.17 |
| Informer | 85.25 | 89.92 | 90.42 | 91.42 |
| GAT | 79.58 | 82.42 | 84.83 | 90.58 |
| CAEMRAB-E | 90.75 | 93 | 92 | 93.75 |
| CAEMRAB-P | 88 | 85.08 | 89 | 90.75 |

## 4 Discussions

Under the operating conditions of heavy load and time-varying speed, traditional CAE models face significant limitations in effectively handling long time-series data. To address this challenge, a multi-head attention mechanism is first introduced after CAE feature extraction to emphasize critical information within the features. Second, residual connections are employed to enhance the transmission of feature information and mitigate the loss of valuable information during training. Finally, by incorporating a BiLSTM model, which is particularly effective for long sequence modeling, the proposed framework achieves comprehensive processing of temporal features. These improvements enable the model to extract discriminative features from various sensor signals more effectively than traditional approaches. Comparative experiments further demonstrate that the proposed CAEMRAB feature fusion model achieves higher accuracy and stronger robustness under complex working conditions, thereby laying a solid theoretical foundation for fault diagnosis and operational monitoring of large-scale hydraulic press equipment.

Despite the promising experimental performance, the proposed model still has certain limitations. First, it exhibits a strong reliance on labeled data, while in the operational context of large-scale equipment (as shown in Fig. 1), sufficient fault samples are often difficult to obtain, posing a major challenge for research. Second, the model's complex structure demands considerable computational resources, which limits its applicability for direct industrial deployment.

Future research will focus on addressing these issues of data scarcity and model complexity. Specifically, we will explore small-sample learning and transfer learning

approaches to reduce dependence on large-scale labeled datasets and enhance generalization across different equipment and operating conditions. In addition, further optimization of model architecture and computational efficiency will be pursued to accelerate real-world implementation, thereby improving the engineering value and application potential of the proposed methodology.

# 5 Conclusion

This study proposes a feature fusion model based on CAEMRAB for diagnosing internal leakage faults in hydraulic cylinders under long motion cycles, heavy load, and time-varying operating conditions. The approach leverages multi-source sensor fusion classification, focusing on displacement error and pressure data closely related to fault types, thereby fully demonstrating the advantages of multi-source signal feature fusion. In addition, ablation models, advanced models, single-signal diagnostic models, different data samples, and varying noise environments were employed in comparative experiments to further validate the effectiveness and stability of the proposed model. The main conclusions are summarized as follows:

(a) In this paper, improvements were made to the encoder module of the conventional CAE model, and a semi-supervised feature fusion model based on CAE and augmented with a multi-head self-attention mechanism, residual mechanism, and BiLSTM module was proposed. Through multiple comparative experimental designs, the proposed model achieves at least 3.92% and 4.17% higher accuracy than the ablation models and other advanced models, respectively, effectively demonstrating its strong performance in diagnosing hydraulic cylinder faults under heavy load and time-varying operating conditions.

(b) Diagnostic tests using only displacement error or pressure signals reveal the limitations of single-sensor data in fault diagnosis for the nonlinear hydraulic cylinder motion process. The proposed feature fusion strategy improves diagnostic performance by at least 5.75% compared with single-signal diagnosis.

(c) The proposed model exhibits strong diagnostic stability concerning the scale of labeled data; when the number of labeled data sets increases from 300 to 400, the model's diagnostic accuracy improves by 11.08%.

(d) Under various noise environments, by adding different levels of Gaussian noise to the original experimental noise, the diagnostic performance of the data can reach at least 98.24%, and high diagnostic accuracy is maintained across different noise signals, effectively validating the model's high robustness.

## Author Contribution:

Chen Yang: Writing-original draft, Writing-review & editing, Methodology, Validation, Data curation. Jianwen Yan: Software, Validation, Methodology, Resources. Yixiong Feng: Conceptualization, Methodology. Lei Li: Conceptualization, Methodology, Supervision, Funding acquisition. Jianrong Tan: Methodology.

## Funding Information:

This study was co-supported by the Scientific Research Foundation for High-level Talents of Anhui University of Science and Technology (2024yjrc73), R&D and industrialization of high-precision intelligent forging equipment for forming large-size light alloy components (202423i08050024), and a large die forging press operation condition monitoring sensor and system application (2023YFB3210805)

## Data Availability:

The authors declare that the main data supporting the findings of this study are available within the paper and its Supplementary Information files.

## Conflicts of Interest:

The authors declare no competing interests.

## Dates:

Received 18 August 2025; Accepted 16 March 2026; Published online 31 March 2026

# References

[1] Kumar P, Park S, Zhang Y, Jo, et al. (**2024**). A Review of Hydraulic Cylinder Faults, Diagnostics, and Prognostics [J]. *International Journal of Precision Engineering and Manufacturing-Green Technology* . 11(5), 1637-1661. doi: 10.1007/s40684-024-00639-3.

[2] Qiu Z, Min R, Wang D, et al. (**2022**). Energy features fusion based hydraulic cylinder seal wear and internal leakage fault diagnosis method [J]. *Measurement* . 195, 111042. doi: 10.1016/j.measurement.2022.111042.

[3] Shanbhag V V, Meyer T J J, Caspers L W, et al. (**2021**). Failure Monitoring and Predictive Maintenance of Hydraulic Cylinder State of the Art Review [J]. *IEEE/ASME Transactions on Mechatronics* . 26(6): 3087-3103. doi: 10.1109/TMECH.2021.3053173.

[4] Fu X, Liu B, Zhang Y, et al. (**2014**). Fault diagnosis of hydraulic system in large forging hydraulic press [J]. *Measurement*. 49, 390-396. doi: 10.1016/j. measurement. 2013.12.010.

[5] Liu H, Liu D, Lu C, et al. (**2014**). Fault diagnosis of hydraulic servo system using the unscented kalman filter [J]. *Asian Journal of Control* . 16(9), 1713-1725. doi: 10.1002/asjc.860.

[6] Xu Q N, Lee K M, Zhou H, et al. (2015). Model-Based Fault Detection and Isolation Scheme for a Rudder Servo System [J]. *IEEE Transactions on Industrial Electronics* . 62, 2384-2396. doi: 10.1109/TIE.2014.2361795.

[7] Maddahi A, Kinsner W, Sepehri N. (**2016**). Internal Leakage Detection in Electrohydrostatic Actuators Using Multiscale

Analysis of Experimental Data [J]. *IEEE Transactions on Instrumentation and Measurement* . 65, 2734-2747. doi: 10.1109/TIM.2016.2608446.

[8] Jin Y, Shan C, Wu Y, et al. (**2019**). Fault Diagnosis of Hydraulic Seal Wear and Internal Leakage Using Wavelets and Wavelet Neural Network [J]. *IEEE Transactions on Instrumentation and Measurement* . 68, 1026-1034. doi: 10.1109/TIM.2018.2863418.

[9] Ma D, Liu Z H, Gao Q H, et al. (**2025**). Fault diagnosis of multi-step electromagnetic hydraulic valve group based on localized current signal CS-SVM [J]. *Measurement* . 245, 116632. doi: 10.1016/j.measurement.2024.116632.

[10] Yin H, Xu H, Fan W, et al. (**2024**). Fault diagnosis of pressure relief valve based on improved deep Residual Shrinking Network [J]. *Measurement* . 224, 113752. doi: 10.1016/j. measurement.2023.113752.

[11] Zhang S, Liang W H, Zhao W Z, et al. (**2024**). Electro-hydraulic SBW fault diagnosis method based on novel 1DCNN-LSTM with attention mechanisms and transfer learning [J]. *Mechanical Systems and Signal Processing* . 220, 111644. doi: 10.1016/j.ymssp.2024.111644.

[12] Liao W, Fu W, Yang K, et al. (**2024**). Multi-scale residual neural network with enhanced gated recurrent unit for fault diagnosis of rolling bearing [J]. *Measurement Science and Technology* . 35, 056114. doi: 10.1088/1361-6501/ad282a.

[13] Zou L, Zhuang K J, Zhou A, et al. (**2023**). Bayesian optimization and channel-fusion-based convolutional autoencoder network for fault diagnosis of rotating machinery [J]. *Engineering Structures* . 280, 115708. doi: 10.1016/j. engstruct.2023.115708

[14] Li Xin, Ma Z, Yuan Z, et al. (**2024**). A review on convolutional neural network in rolling bearing fault diagnosis [J]. *Measurement Science and Technology* . **35,** 072002. doi: 10.1088/1361-6501/ad7a91.

[15] Nguyen T P, Cho M Y. (**2024**). Advanced AIoT for failure classification of industrial diesel gener-ators based hybrid deep learning CNN-BiLSTM algorithm [J]. *Advanced Engineering Informatics* . 62, 102644. doi: 10.1016/j. aei.2024.102644.

[16] Liu Y, Li W, Lin S, et al. (**2023**). Hydraulic system fault diagnosis of the chain jacks based on multi-source data fusion [J]. *Measurement* . 217, 113116. doi: 10.1016/j. measurement.2023.113116.

[17] Dao F, Zen Y, Qian J. (**2024**). Fault diagnosis of hydro-turbine via the incorporation of bayesian algorithm optimized CNN-LSTM neural network [J]. *Energy* . 290, 130326. doi: 10.1016/j.energy.2024.130326.

[18] Ma Z, Sun Y W, Ji H, et al. (**2024**). A CNN-BiLSTM-Attention approach for EHA degradation prediction based on time-series generative adversarial network [J]. *Mechanical Systems and Signal Processing* . 215, 111443. doi: 10.1016/j. ymssp.2024.111443.

[19] Liang P F, Wang X F, Ai C, et al. (2025). SRSGCN: A novel multi-sensor fault diagnosis method for hydraulic axial piston pump with limited data [J]. *Reliability Engineering & System Safety* . 253, 110563. doi: 10.1016/j.ress.2024.110563.

[20] Snyder Q, Jiang Q, Tripp E. (**2025**). Integrating self-attention mechanisms in deep learning: A novel dual-head ensemble transformer with its application to bearing fault diagnosis [J]. *Signal Processing* . 227, 109683. doi: 10.1016/j. sigpro.2024.109683.

[21] Wang W Y, Zuo E G, Chen C, et al. (**2025**). Efficient time series adaptive representation learning via dynamic routing sparse attention [J]. *Pattern Recognition* . 158, 111058. doi: 10.1016/j.patcog.2024.111058.

[22] Zeng L, Jin Q, Li Z, et al. (**2024**). Dual-attention LSTM autoencoder for fault detection in industrial complex dynamic processes [J]. *Process Safety and Environmental Protection* . 185, 1145-1159. doi: 10.1016/j.psep.**2024**.02.042.

[23] Dong Y, Jian H, Jiang W, et al. (**2024**). Dynamic normalization supervised contrastive network with multiscale compound attention mechanism for gearbox imbalanced fault diagnosis [J]. *Engineering Applications of Artificial Intelligence* . 133, 108098. doi: 10.1016/j. engappai. 2024.108098.

[24] Huang X, Xie T, Wu J, et al. (**2024**). Deep continuous convolutional networks for fault diagnosis [J]. *Knowledge-Based Systems* . 292, 111623. doi: 10.1016/j. knosys.2024.111623.

[25] Zhang Y, Ji J, Ma B. (**2020**). Fault diagnosis of reciprocating compressor using a novel ensemble empirical mode decomposition-convolutional deep belief network [J]. *Measurement* . 156, 107619. doi: 10.1016/j. measurement. 2020.107619.

[26] Zhang Y, Huang B Y, Xin Q, et al. (**2022**). Ewtfergram and its application in fault diagnosis of rolling bearings [J]. *Measurement* . 190, 110695. doi: 10.1016/j. measurement.2021.110695.

[27] Chen Q, Yao Y, Gui G, et al. (**2022**). Gear Fault Diagnosis Under Variable Load Conditions Based on Acoustic Signals [J]. *IEEE Sensors Journal* . 22, 22344-22355. doi: 10.1109/ JSEN.2022.3214286.

[28] Huang K, Wu S, Li F, et al. (**2022**). Fault Diagnosis of Hydraulic Systems Based on Deep Learning Model with Multirate Data Samples [J]. *IEEE Transactions on Neural Networks and Learning Systems* . 33, 6789-6801. doi: 10.1109/TNNLS.2021.3083401.

[29] Guan H, Ren Y, Tang H, et al. (**2024**). Intelligent fault diagnosis methods for hydraulic components based on information fusion: review and prospects [J]. *Measurement Science and Technology* . 35, 082001. doi: 10.1088/1361-6501/ad437e.

[30] Shi J, Yi J, Ren Y, et al. (**2021**). Fault diagnosis in a hydraulic directional valve using a two-stage multi-sensor information fusion [J]. *Measurement* . 179, 109460. doi: 10.1016/j. measurement.2021.109460.

[31] Xiao X Q, Li C S, He H G, et al. (**2025**). Rotating machinery fault diagnosis method based on multi-level fusion framework

of multi-sensor information [J]. *Information Fusion* . 113, 102621. doi: 10.1016/j.inffus.2024.102621.

[32] Yang Z K, Li G, Xue G, et al. (**2025**). A novel multi-sensor local and global feature fusion architecture based on multi-sensor sparse transformer for intelligent fault diagnosis [J]. *Mechanical Systems and Signal Processing* . 224 , 112188. doi: 10.1016/j.ymssp.2024.112188.

[33] Li K, Sun Z, Jin H, et al. (**2024**). Semi-supervised diagnosis method of refrigeration compressor hidden defect based on convolutional transformer autoencoder model [J]. *International Journal of Refrigeration* . 158, 47-57. doi: 10.1016/j.ijrefrig.**2023**.10.021.

[34] Zhong Q, Xu E, Shi Y, et al. (**2023**). Fault diagnosis of the hydraulic valve using a novel semi-supervised learning method based on multi-sensor information fusion [J]. *Mechanical Systems and Signal Processing* . 189, 110093. doi: 10.1016/j.ymssp.**2022**.110093.

[35] Tang S, Zhu Y, Yuan S Q. (**2022**). An adaptive deep learning model towards fault diagnosis of hydraulic piston pump using pressure signal [J]. *Engineering Failure Analysis* . 138, 106300. doi: 10.1016/j.engfailanal.**2022**.106300.

[36] Tang S, Zhu Y, Yuan S Q. (**2021**). An improved convolutional neural network with an adaptable learning rate towards multi-signal fault diagnosis of hydraulic piston pump [J]. *Advanced Engineering Informatics* . 50, 101406. doi: 10.1016/j.aei.**2021**.101406.

[37] Honkela T, Duch W, Girolami M, et al. (**2011**). Artificial Neural Networks and Machine Learning - ICANN 2011: 21st International Conference on Artificial Neural Networks, Espoo, Finland, Proceedings, Part I, Lecture Notes in Computer Science. *Springer Berlin Heidelberg, Berlin, Heidelberg* . doi: 10.1007/978-3-642-21735-7.

[38] Ding L, Li Q. (**2024**). Fault diagnosis of rotating machinery using novel self-attention mechanism TCN with soft thresholding method [J]. *Measurement Science and Technology* . 35, 047001. doi: 10.1088/1361-6501/ad1eb3.

[39] Vo T T, Liu M K, Tran M Q. (**2024**). Harnessing attention mechanisms in a comprehensive deep learning approach for induction motor fault diagnosis using raw electrical signals [J]. *Engineering Applications of Artificial Intelligence* . 129, 107643. doi: 10.1016/j.engappai.**2023**.107643.

[40] Wang S, Tian J, Liang P, et al. (**2024**). Single and simultaneous fault diagnosis of gearbox via wavelet transform and improved deep residual network under imbalanced data [J]. *Engineering Applications of Artificial Intelligence* . 133, 108146. doi: 10.1016/j.engappai.**2024**.108146.

[41] Han S, Sun S, Zha Z, et al. (**2024**). Deep Residual Multiscale Convolutional Neural Network With Attention Mechanism for Bearing Fault Diagnosis Under Strong Noise Environment [J]. *IEEE Sensors Journal* . 24, 9073-9081. doi: 10.1109/JSEN.2023.3345400.

[42] Sun Z, Yang H, Fang M, et al. (**2024**). On Bayesian Optimization-Based CNN-BiLSTM Network for Multiclass Classification in Distributed Optical Fiber Vibration Sensing Systems [J]. *IEEE Transactions on Instrumentation and Measurement* . 73, 7006414. doi: 10.1109/TIM.**2024**.3451576.

[43] Chen Y J, Wang J L, Chen W D, et al. (**2024**). Fault diagnosis in hydropower units based on chaotic Kepler optimization algorithm-enhanced BiLSTM model [J]. *Energy Reports* . 12, 5163-5176. doi: 10.1016/j.egyr.**2024**.11.008.

[44] Bi C, Yue X K, Dang Z H, et al. (**2025**). A dynamic fault diagnosis method for gravitational reference sensor based on informer-RS [J]. *IEEE Sensors Journal* . 25, 3982-3997. doi: 10.1109/JSEN.2024.3510739.